Constraining Beyond the Standard Model Sub-MeV Neutrino Fluxes Using the XENONnT Detector

Amy Flather,[1] Noah Chavez,[2] and Ian M. Shoemaker[3]

[1]*Rutgers University, Piscataway, NJ, USA*
[2]*Amherst College, Amherst, MA, USA*
[3]*Center for Neutrino Physics, Department of Physics, Virginia Tech University, Blacksburg, VA 24601, USA*

Although naturally occurring neutrino fluxes have been observed across a range of energies, none have been detected below the MeV-scale. These same energy scales are often probed by dark matter direct detection experiments like XENONnT. XENONnT measures electron recoil events with sensitivity in the 1-30keV range and recently agreed with the predicted Standard Model background event rate. However, this data can be repurposed as a method of constraining a Beyond the Standard Model (BSM) low-energy neutrino flux. Here, we extract the first sub-MeV model-independent neutrino flux bounds using the latest experimental data from XENONnT. We place BSM flux constraints on the order of $10^5 (\mathrm{cm}^2\,\mathrm{s}\,\mathrm{eV})^{-1}$ (90% C.L.) for neutrinos at energies from 16keV to 1.8MeV. These flux bounds constrain new regions of parameter space and are relevant for models of decaying dark matter and decaying primordial black holes. Our results illustrate how the high sensitivity of dark matter direct detection experiments can be used to constrain neutrino fluxes. We expect this work to apply to other dark matter direct detection experiments.

Introduction

Neutrino fluxes and their sources exist across a wide range of energies and have been combined into the Grand Unified Neutrino Spectrum (GUNS). The current GUNS, shown in Fig. 1, covers a range of neutrino energies from the MeV scale with solar neutrinos to the highest PeV neutrinos with extra-galactic neutrinos [1]. However, while the Standard Model (SM) predicts several fluxes below the MeV scale, including thermal solar neutrinos and the Cosmic Neutrino Background, none have been detected thus far due to limited detector sensitivity. Neutrino detectors typically operate at higher energies, and there has not been significant motivation to build a neutrino detector at such low energies due to the fact that the neutrino cross section decreases as a function of energy, which makes the sub-MeV neutrinos increasingly difficult to detect and study.

However, despite these complications, this unexplored sub-MeV neutrino energy region is of particular interest to Beyond the Standard Model (BSM) physics. The discovery of neutrino oscillations showed that, contradictory to the SM, neutrinos have mass and therefore require BSM physics. Since then, many possible models have been proposed, including those that predict neutrino fluxes from various hypothetical new sources. These sources include decaying dark matter models as well as decaying primordial black holes, and predict neutrino fluxes below the MeV scale [2]. But unless we are able to detect sub-MeV neutrinos, it is not possible to use experimental data to constrain these BSM models, which is a necessary step for BSM physics searches.

Fortunately, certain dark matter direct detection experiments have the required sensitivity and capability to probe for sub-MeV neutrinos. Since dark matter has very low energies, in order to see it directly, detectors must be sensitive to very low energy events. One of these detectors is the XENONnT dark matter experiment, which is an 8.5 tonne liquid xenon (Xe) detector used to search for Weakly Interacting Massive Particles (WIMPs) [3]. XENONnT detects light from the collisions of incoming particles with Xe atoms in the detector volume. The incoming particles can collide with either the electrons or the nucleus of the Xe atoms, called electron or nuclear recoils, respectively. In both recoil cases, the particle will cause the electron or nucleus to recoil with a certain energy, thus emitting photons that can be detected with photomultipliers on the edges of the detector. XENONnT can see recoils down to 1keV in energy. However, the recoil energies seen by the detector are not proportional to the energy of the incoming particle, but instead depend on the mass ratio between the particle and the target. A more massive particle at a given kinetic energy will cause an electron or nucleus to recoil with more energy than a less massive particle. Similarly, since the electron has a smaller mass than a Xe nucleus, a particle with a fixed mass and energy will cause higher energy electron recoils than nuclear recoils.

There are many different types of particles that can produce electron or nuclear recoils, including WIMPs and other hypothetical dark matter particles, but neutrinos also produce these recoils. Therefore, we can repurpose the XENONnT dark matter experiment to instead constrain low-energy neutrino fluxes. Even though these low-energy fluxes are well-predicted by both the SM and various BSM physics, we assume that they are model-independent in our calculations.

In this paper, we present the first constraints on sub-MeV neutrino fluxes using the XENONnT detector. XENONnT can see down to 16keV neutrinos with electron recoils and down to 7.82MeV neutrinos with nuclear recoils. Since the electron recoils cover a broader energy range than the nuclear recoils, we choose to focus on the

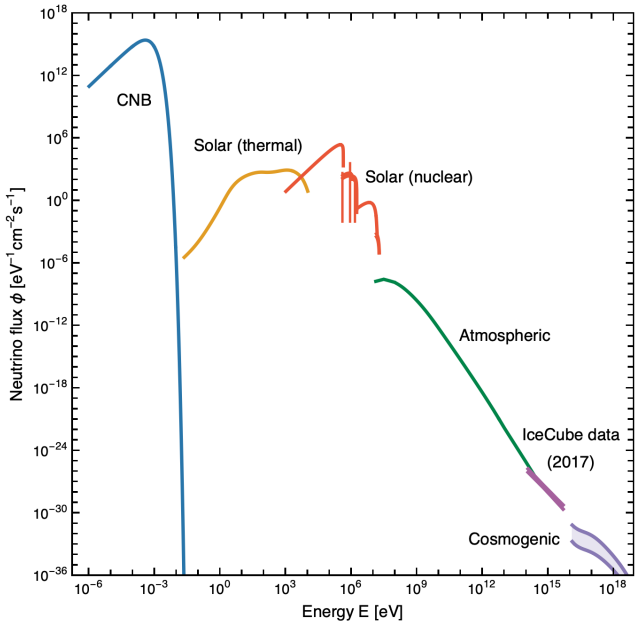

FIG. 1: A plot of the Grand Unified Neutrino Spectrum (GUNS) [1]. There are a variety of SM neutrino sources, that span a wide range of energies. However, no fluxes below $1.8 \cdot 10^6$eV have been experimentally detected.

former type in this paper.

This paper is structured as follows: we first present our methodology for calculating the neutrino flux constraints in the sub-MeV region from 16keV to 1.8MeV, then proceed to show our constraint results superimposed with the current GUNS plot from Fig. 1, and finally finish with remarks on the applicability of this work to other detectors, as well as the feasibility of using dark matter direct detection experiments to measure sub-MeV SM neutrino fluxes.

Methodology: Calculating neutrino flux constraints

Experimental data from XENONnT allows for model-independent neutrino flux constraints to be obtained through statistical model comparisons [4, 5]. Our approach can be viewed as a three-step process. First, we define some BSM neutrino flux of arbitrary strength and attach a scaling pre-factor to it. Second, we calculate the event rate that XENONnT would hypothetically measure from this BSM flux. Lastly, we scale the initial BSM flux we created and use a statistical model comparison test to determine at what strength the recoil events generated from this new flux exceed a 90% confidence level relative to the SM background. In addition to determining flux constraints from data using XENONnT, we also consider hypothetical constraints from future experiments with different thresholds and exposures. In this section we describe our methods to obtain flux limits from current and future detectors.

A. BSM neutrino flux limits from XENONnT

A general method to obtain a recoil event rate for a detector is to integrate over the product of a differential neutrino flux, the neutrino-electron cross section, and the target density of the detector [4, 6]. This relationship can be written as

$$\frac{dR}{dE_R} = N_T \int_{E_\nu^{min}} \frac{d\sigma}{dE_R} \frac{dN_\nu}{dE_\nu} dE_\nu, \tag{1}$$

where $\frac{dR}{dE_R}$ is recoil event rate, N_T is the number of targets per kg, $\frac{d\sigma}{dE_R}$ is the neutrino-electron cross section, and $\frac{dN_\nu}{dE_\nu}$ is a differential neutrino flux. Both target density and cross section are known quantities that correspond to experimental attributes [3, 4]. Therefore, to obtain an event rate, the only unknown we will manipulate is the neutrino flux. Since we aim to develop a model-independent constraint, we are free to create any flux, but in this work, we focus on the sub-MeV energy region in an effort to constrain various BSM models such as decaying primordial black holes [7].

Recall that to calculate the flux constraints we must determine the strength at which a given hypothetical flux must be to generate an increase in events large enough to statistically deviate from the SM background. It then follows that we must add a pre-factor onto whatever flux we create so that it can be scaled to find the limits. In this work, we primarily consider limits using box function- and Dirac delta function-shaped fluxes. As an example, to set a constraint at neutrino energy a we would create a delta function flux of the form

$$\frac{dN_\nu}{dE_\nu} = \phi\, \delta(E_\nu - a), \tag{2}$$

where ϕ is a scaling pre-factor. For the box function, we constrain a range of energies equal to the width of the function.

Before we can obtain the event rate for the BSM neutrino flux we have created, we must also consider the sensitivity of the detector we intend to use. Here, we use XENONnT, which detects electron recoils with varying sensitivity as a function of recoil energy [3]. Incorporating this dimensionless efficiency function, which we name $\mathcal{E}(E_R)$, we find that XENONnT will measure

$$\frac{dR(E_R)}{dE_R} = \mathcal{E}(E_R)\, N_T \int_{E_\nu^{min}} \frac{d\sigma(E_\nu, E_R)}{dE_R} \frac{dN_\nu(E_\nu)}{dE_\nu} dE_\nu \tag{3}$$

as its BSM flux event rate. The efficiency function of XENONnT approaches zero around 1keV electron recoils, and therefore the minimum neutrino energy required is about 16keV. We obtain this energy using the equation

$$E_\nu^{\min} = \frac{1}{2}\left(E_R + \sqrt{E_R(E_R + 2m_e)}\right) \tag{4}$$

where m_e is the mass of an electron [4, 6]. We assume a neutrino mass of zero. Upon the substitution of Eq. (2)

into Eq. (3), we obtain the event rate from our BSM flux we created.

With the event rate calculated, we now move onto the statistics of setting a constraint. We employ a binned maximum log-likelihood method that functions as a modified chi squared model comparison test [8]. Maximizing the likelihood is equivalent to minimizing the left hand side in the equation

$$\underbrace{-2\ln\lambda(\theta)}_{\chi^2} = 2\sum_{i=1}^{N}\left[\mu_i(\theta) - n_i + n_i \ln\frac{n_i}{\mu_i(\theta)}\right], \qquad (5)$$

where μ_i is the number of theoretical events per bin and n_i is the number of events measured per bin by XENONnT. We obtain our values for n_i using the most recent experimental data from XENONnT, which has been provided for use by the XENON collaboration [3]. We choose to name the left hand side of Eq. (5) as χ^2 because it acts as a χ^2 value from the familiar chi-squared test throughout our analysis. That is, we use the left hand side of Eq. (5) as a value in a χ^2 distribution and compare it to some critical value corresponding to a given confidence level.

However, to perform this method we must transform our event rate into a dimensionless event count. We choose to create 30 bins of 1 keV width and integrate over all event rates to obtain the number of events. This work considers a hypothetical BSM neutrino flux event rate in addition to the predicted SM background event rate, B_0, as shown in Fig. 2 so for μ_i we have

$$\mu_i = 1.16\int_i^{i+1}\left[\phi\left(\frac{dR(E_R)}{dE_R}\right) + B_0(E_R)\right]dE_R, \qquad (6)$$

where i is the lowest energy of a bin and $i+1$ is the greatest. The SM background, B_0, and experiment exposure of 1.16 tonne-years are given by the XENON collaboration [3]. We include the exposure of 1.16 tonne-years because the event rate will have units of (tonne yr keV)$^{-1}$, and the integral will only eliminate the keV. Note that our scaling pre-factor, ϕ, is attached to just the BSM event rate and not the SM background term. Now that we have our dimensionless event counts, we can proceed with our statistical analysis.

Since we are constraining a BSM flux using the SM as our background we perform a model comparison test,

$$\Delta\chi^2 = \chi^2_{\rm BSM} - \chi^2_{\rm SM} = 2.71, \qquad (7)$$

where 2.71 comes from the critical value for a 90% confidence level [8]. The value of ϕ that solves Eq. (7) multiplied by the strength of the initial BSM flux created is the model-independent neutrino flux constraint. Fig. 2 illustrates how the 90% C.L BSM event rate generates a significant amount of excess events over the SM event rate. It is important to note that for $\chi^2_{\rm SM}$ the BSM event rate is zero, so the calculation of μ_i in Eq. (6) is simplified by setting the first term in the integrand to zero.

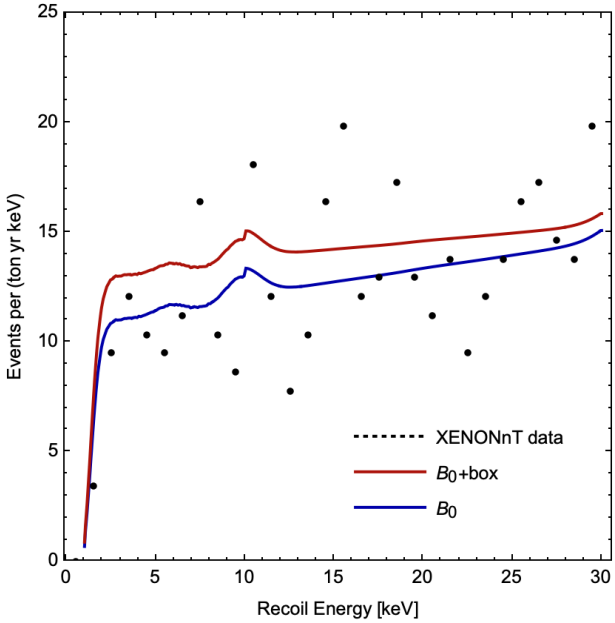

FIG. 2: Event rates from the 90% C.L BSM flux and the SM background flux, B_0, are shown. In addition, experimental data from XENONnT is plotted. It can easily be seen that the BSM event rate is significantly larger than the SM rate, demonstrating that the BSM event rate corresponds to a flux limit.

B. Future experiments and solar thermal flux

In this work we also consider how flux limits may differ as future experiments come online with improved thresholds and exposures. By taking future experiments into account we are also able to determine what exposure is required to detect low-energy SM predicted fluxes like the solar thermal flux.

One aspect we investigate is how flux limits will evolve under a change to detector threshold, which requires adjustments to our previous method. Our first step is to translate the efficiency function, $\mathcal{E}(E_R)$, to lower energies. Today, XENONnT operates at a threshold of 1 keV so to set the threshold to 0.5keV, the efficiency function becomes $\mathcal{E}(E_R - 0.5)$ [3]. However, to extract a flux constraint using Eq. (5) we require both experimental data and a SM background event rate which are not available below 1keV due to XENONnT's current threshold preventing measurement of any events. This forces us to extrapolate the background to lower energies. We assume that the background retains the strength it was at before suppressed by the threshold, and extend the curve to lower energies as shown in Fig. 3. To account for the lack of experimental data below the current threshold, we assume the data will be in perfect agreement with the SM background with no added noise. Together with the extrapolated SM background event rate we can again use Eq. (5) to obtain constraints, but now for lower thresholds to investigate the constraining potential of future

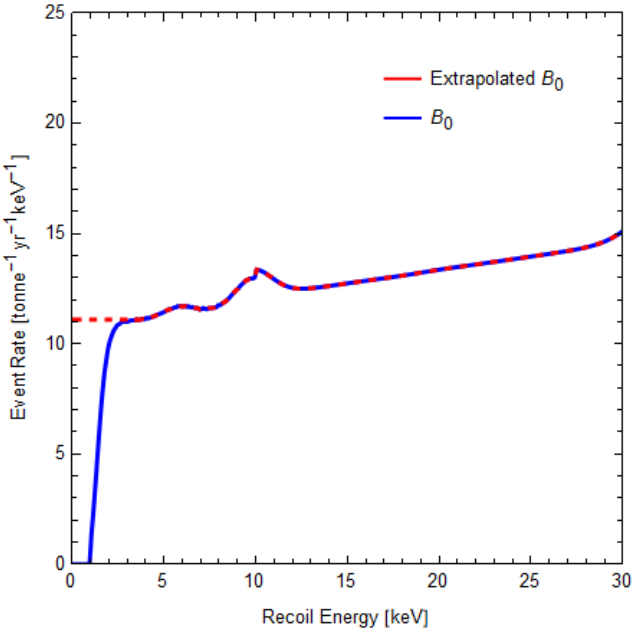

FIG. 3: The SM background event rate, B_0, and extended SM background event rate are shown. Our analysis of future constraints requires an extrapolated background curve. To extrapolate to lower energies, we assume the event rate remains constant at energies lower than the current threshold of 1keV.

liquid xenon experiments.

The ability to investigate potential constraints arising from future lower threshold liquid xenon detectors also allows this work to determine the exposure required at a given threshold to observe the SM predicted, but not yet observed, solar thermal flux as seen in Fig. 1 [1]. The exposure is easily manipulated by altering the coefficient in front of the integral in Eq. (6). We elaborate more on this process and outcome in the next section.

We acknowledge that in our consideration of future experiments and different exposures we make many significant assumptions. We intend for this methodology to provide preliminary results and serve as a proof of concept in considering how future detectors may perform.

Results

In this section, we present our model-independent sub-MeV neutrino flux constraints. In their paper, XENONnT provided neutrino recoil data from 1keV to 30keV [3], which limits our constraints to neutrino energies from 16keV to 1.8MeV. We divide this energy region into equally-spaced box function fluxes and perform the significance calculation on each flux individually, yielding a differential flux constraint with units of $(\mathrm{cm}^2\,\mathrm{s\,eV})^{-1}$ for each box. Then, we combine each of the individual constraints for each box into one constraint curve to produce the total constraint over the full energy region. Our choice of the width of the box function was arbitrary, thus we consider nine widths ranging from 10keV to 1MeV, creating one curve per width, and observe how this change effects our final constraints. The results of each of these nine constraint curves is summarized in Fig. 4. For the smallest bin width of 10keV, our constraints are of order $10^6(\mathrm{cm}^2\,\mathrm{s\,eV})^{-1}$, while for the largest bin width of 1MeV, our constraints are of order $10^5(\mathrm{cm}^2\,\mathrm{s\,eV})^{-1}$. We can therefore see that the constraint curve is largely dependent on the choice of the box flux bin width. Smaller widths yield a weaker constraint that decreases as neutrino energy increases, while larger widths yield a stronger constraint that is more constant as neutrino energy increases.

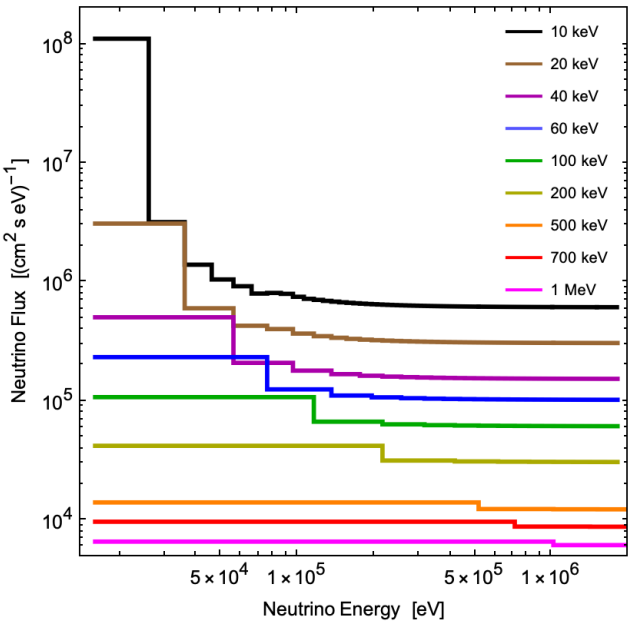

FIG. 4: The constraints on neutrino fluxes from 16keV to 1.8MeV assuming box function neutrino fluxes. We considered 9 different widths from 10keV to 1MeV, each shown in a different color.

Next, we consider breaking the 16keV-1.8MeV energy region into fluxes with a width of zero, or more precisely, into Dirac delta function fluxes. We perform the significance calculation for delta function fluxes spaced 10keV apart in the energy region, and interpolate our constraint curve to fill in the gaps for the remaining values between the given energies. Our constraint curve is summarized in Fig. 5, which gives the total flux instead of the differential flux calculated for the box function fluxes. For comparison, the 100keV box function constraint curve is included in Fig. 5 as well, but in units of total flux, $(\mathrm{cm}^2\,\mathrm{s})^{-1}$, instead of units of differential flux, $(\mathrm{cm}^2\,\mathrm{s\,eV})^{-1}$. To convert between these two units, we multiplied each of the constraint values for the 100keV curve in Fig. 4 by 100keV.

Finally, we return to the GUNS in Fig. 1 to determine how our constraint values compare to known and

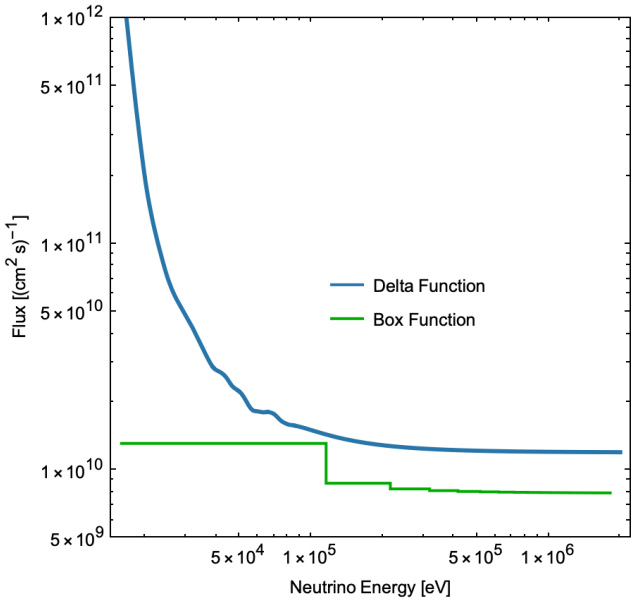

FIG. 5: Constraint on neutrino fluxes assuming a delta function flux shape. For comparison, the 100keV width box function constraint from Fig. 4 shown as well. The units in this plot are in total flux instead of the differential flux units used for the constraints from the box function fluxes.

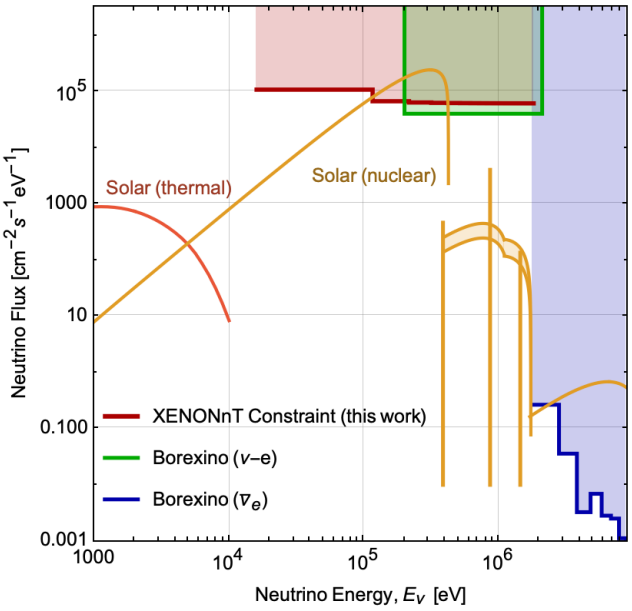

FIG. 6: The Grand Unified Neutrino Spectrum with our 100keV width constraint from XENONnT overlaid. This plot is a rescaled version of the plot in Fig. 1, with only the solar thermal flux and the solar nuclear visible. The previous lowest energy limits from the Borexino detector are shown in green and blue. Our constraints cover an additional order of magnitude compared to previous experiments.

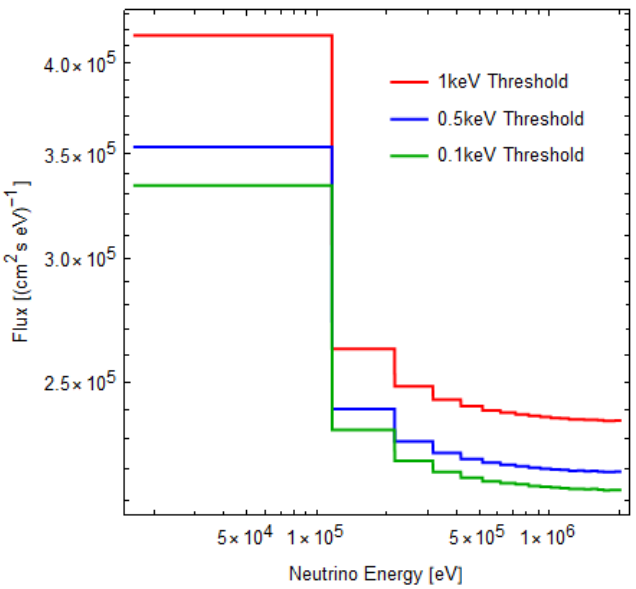

FIG. 7: Neutrino flux constraints for a 100keV width box function for three different threshold values: the original 1keV, 0.5keV and 0.1keV.

predicted neutrino fluxes within the sub-MeV energy region. We again choose the 100keV bin width box function constraint plot and overlay it onto the GUNS spectrum in Fig. 6. In addition, we have added BSM neutrino flux constraints from the Borexino detector for comparison, the previous lowest energy constraints [9]. We can see that our BSM neutrino flux constraints, while slightly weaker than Borexino's in the MeV region where they overlap, cover a new order of magnitude between 10^4 eV and $2 \cdot 10^5$ eV. These preliminary results are the first step in constraining or ruling out possible BSM models that predict sub-MeV neutrino fluxes.

As an extension to finding model-independent flux constraints using current XENONnT data, we also consider how the flux constraints may change for future experiments. Specifically, we expect future experiments to have a lower threshold as detector technology improves, resulting in stronger constraints as threshold decreases due to the additional recoil events that can be measured by the detector. We calculated the flux constraints for thresholds of 0.5keV and 0.1keV and plotted them together with the current 1 keV threshold XENONnT curve in Fig. 7. As expected, the threshold of 0.1keV provides the strongest constraints. It is also the case that the constraint improvement is not uniform across neutrino energies. Instead, the constraint becomes proportionally stronger at lower neutrino energies than at higher ones, suggesting that a lower threshold would provide particularly strong constraints for lower-energy neutrino fluxes.

Furthermore, we can use these results to predict the exposure needed to detect SM neutrino fluxes predicted in this energy region. The current XENONnT detector has an exposure thus far of 1.16 tonne-years, so we expect our future exposure to be significantly higher than this value. We focus on the thermal solar neutrino flux, given that this is the highest energy flux below the MeV range

that has not been detected. Instead of assuming a box function shape as a constraint for the thermal neutrino flux, we take it to be the same shape as predicted by the GUNS. We assume optimistically an efficiency of 1, background rate of 0, and threshold of 0.1keV, meaning we are able to see all recoils within the detector volume and all recoil events that are seen come from the thermal solar flux and not from other unrelated sources. We estimate that in order to detect one recoil event from the thermal solar flux, an experiment needs an exposure of $1 \cdot 10^6$ tonne-years. Note that the choice to scale the solar thermal flux itself and find the exposure required for only one event is a different approach than used for our other constraints. This exposure is significantly greater than any current neutrino detector, and thus we conclude that, while theoretically possible, it will be practically very difficult to detect thermal solar neutrinos with a liquid xenon detector due to the limited amount of Xe on Earth.

Conclusions

In this paper we investigate using experimental data from XENONnT as a tool to obtain model-independent neutrino flux constraints. We focus on sub-MeV flux constrains because various BSM models like decaying primordial black holes and decaying dark matter predict a low-energy neutrino flux [7]. XENONnT's search for dark matter results in a high sensitivity to electron recoils in the $(1-30)$keV range, allowing for sub-MeV BSM neutrino flux constraints to obtained for the first time [4, 5].

Using hypothetical box and delta function neutrino fluxes in addition to a statistical model comparison test, we apply model-independent neutrino flux constraints in the previously unexplored 16keV-1.8MeV energy region [8]. Moreover, we consider how these constraints improve in future experiments by manipulating the allowed threshold of the detector as well as its exposure time. We find that lower thresholds provide stronger constraints, with the best improvements at lower energies. In considering how a future experiment would perform, we also find that an exposure of 10^6 tonne-years, at a 0.1keV threshold with no background and efficiency of 1, is required to detect one event from the solar thermal flux using a liquid xenon detector [1]. We intend for our results on future experiments to be purely preliminary and acknowledge that we make significant assumptions.

Lastly, since no neutrino fluxes have been detected in the sub-MeV region, including the SM predicted solar thermal flux, this work demonstrates how dark matter direct detection experiments provide the ability to constrain previously unattainable energies. We anticipate that these methods extend to other sensitive DM detectors like SENSEI [10]. Moreover, this work has shown that continuing to improve the sensitivity and exposure of DM direct detection experiments offers valuable results not only to DM searches but also to model-independent neutrino flux constraint efforts.

Acknowledgments

We are grateful to the Virginia Tech REU program for support. This work was supported by the NSF with the award number PHY-2149165. The work of IMS is supported by DOE under the award number DE-SC0020250.

[1] E. Vitagliano, I. Tamborra, and G. Raffelt, Rev. Mod. Phys. **92**, 45006 (2020), arXiv:1910.11878 [astro-ph.HE] .
[2] D. McKeen, Phys. Rev. D **100**, 015028 (2019), arXiv:1812.08178 [hep-ph] .
[3] E. Aprile *et al.* (XENON), Phys. Rev. Lett. **129**, 161805 (2022), arXiv:2207.11330 [hep-ex] .
[4] T. Schwemberger and T.-T. Yu, Phys. Rev. D **106**, 015002 (2022), arXiv:2202.01254 [hep-ph] .
[5] R. Essig, M. Sholapurkar, and T.-T. Yu, Phys. Rev. D **97**, 095029 (2018), arXiv:1801.10159 [hep-ph] .
[6] J. Billard, L. Strigari, and E. Figueroa-Feliciano, Phys. Rev. D **89**, 023524 (2014), arXiv:1307.5458 [hep-ph] .
[7] R. Calabrese, M. Chianese, D. F. G. Fiorillo, and N. Saviano, Phys. Rev. D **105**, L021302 (2022), arXiv:2107.13001 [hep-ph] .
[8] R. L. Workman *et al.* (Particle Data Group), PTEP **2022**, 083C01 (2022).
[9] M. Agostini *et al.* (Borexino), Astropart. Phys. **125**, 102509 (2021), arXiv:1909.02422 [hep-ex] .
[10] L. Barak *et al.* (SENSEI), Phys. Rev. Lett. **125**, 171802 (2020), arXiv:2004.11378 [astro-ph.CO] .